Journal of Sound and Vibration 329 (2010) 1460–1479

Contents lists available at ScienceDirect

Journal of Sound and Vibration

journal homepage: www.elsevier.com/locate/jsvi

Identification of dynamic characteristics of nonlinear joint based on the optimum equivalent linear frequency response function

H. Kashani [1], A.S. Nobari *

Aerospace Department & Centre of Excellence in Computational Aerospace Engineering, Amirkabir University of Technology, Hafez Ave., Tehran, Iran

ARTICLE INFO

Article history:
Received 2 February 2009
Received in revised form
9 September 2009
Accepted 4 November 2009
Handling Editor: C.L. Morfey
Available online 6 December 2009

ABSTRACT

Identification of dynamic characteristics of local nonlinearities has been aimed in this paper. The spirit of the identification method is established on Optimum Equivalent Linear Frequency response function (OELF). Dynamic behavior of nonlinear elements in system is extracted from OELF using two different techniques. The first technique is "Direct Identification Method" (DIM) in which no pre-assumed model is considered for the nonlinearity's behavior and the second technique is "Model based Identification Method" (MIM). The second technique is introduced with two different formulations, in order to take into account the practical limits due to the inaccessibility of nonlinearity location and/or indeterminability of degree of freedom. Dynamic characteristics of common nonlinearity mechanisms like cubic stiffness, pure slip, and stick-slip have been identified using the proposed technique and it has been shown that, although the proposed identification technique is simple, it does not require any sophisticated measurement hardwares and techniques, as required by most of the identification methods proposed so far. Also, the relation of this technique to harmonic balance method is discussed.

1. Introduction

With continual interest to expand the performance envelope of structures at ever increasing speeds, there is the need for designing lighter, more flexible, and hence more nonlinear structures, and consequently, less safety factors are allowed in the design process. This brings about the need to produce more accurate and high fidelity FE models that can faithfully represent the real system. On the other hand, one of the most difficult tasks in producing accurate FE models is to model the joints properly. This is so because joints are localized elements with predominantly nonlinear and frequency dependent dynamic characteristics. The only reliable method for successful modeling of joints is to identify their mechanical characteristics and incorporate them in the FE model.

There are several published works on identification techniques. These works can be divided into two broad categories namely, 1—identification techniques assuming linear dynamic behavior for joint [1–6] and, 2—identification techniques assuming nonlinear behavior for joint [7–21]. Almost all of the techniques used in second category are based on the very controlled measurements and use some sort of pre-assumed model for the joint behavior.

The main goal of the present work is to propose a nonlinear joint identification method that: (a) does not depend on the sophisticated measurement hardwares and techniques and (b) can be used without any pre-assumption on the joint

* Corresponding author. Tel.: +98 2164543208.
E-mail addresses: h-kashani@aut.ac.ir (H. Kashani), SAL1358@aut.ac.ir, andishan.pars@gmail.com (A.S. Nobari).
[1] Tel.: +98 2164543220.

0022-460X/$ - see front matter © 2009 Elsevier Ltd. All rights reserved.
doi:10.1016/j.jsv.2009.11.007

Nomenclature

CF	constraint-free
CP	connectivity pattern
CS	cubic stiffness
DoF	Degree of Freedom
FE	finite element
FEM	finite element method
FRF	frequency response function
HBM	harmonic balance method
MAC	modal assurance criteria
NLSRM	nonlinear single resonant mode
OELF	optimum equivalent linear FRF
OELI	optimum equivalent linear impedance
PS	pure slip
RMS	root mean square
SL	specified location
SM	symmetric
SS	stick-slip
TD	time domain
$\mathbf{A}$	coefficient matrix of final equation before weighting
$\mathbf{B}$	constant vector of final equation before weighting
$\mathbf{C}$	viscous damping matrix
$\mathbf{C}_n$	nonlinear viscous damping
$E[\cdot]$	expected value
$\mathbf{F}$	Fourier transform of $\mathbf{f}$
$\mathbf{G}$	perturbing function
$\mathbf{H}_l$	underlying linear system FRF
$\mathbf{H}_n$	nonlinear system FRF
$\mathbf{H}_o$	OELF of nonlinear system
$\mathbf{K}$	linear stiffness matrix
$K_{3_{ij}}$	cubic stiffness between nodes i and j
$\mathbf{K}_n$	nonlinear stiffness matrix
$K_{s_{ij}}$	stiffness of Jenkin's element between nodes i and j
$\mathbf{M}$	mass matrix
$\mathbf{P}$	coefficient matrix of final equation after weighting
$P_{s_{ij}}$	pure slip friction force between nodes i and j
$\mathbf{Q}$	constant vector of final equation after weighting
$\mathbf{S_{ff}}$	auto-spectrum of input force
$\mathbf{S_{xx}}$	auto-spectrum of signal $\mathbf{x}$
$\mathbf{S}_{\mathbf{x}_n\mathbf{f}}$	input–output cross-spectrum
$S_{s_{ij}}$	stick-slip friction force of Jenkin's element between nodes i and j
T	sampling period
$\mathbf{X}_n$	Fourier transform of $\mathbf{x}_n$
$\mathbf{X}_o$	Fourier transform of $\mathbf{x}_o$
$\mathbf{Z}$	nonlinearity's impedance
$\mathbf{Z}_{j,:}$	jth row of matrix $\mathbf{Z}$
$\mathbb{Z}$	vector form of matrix $\mathbf{Z}$
$\mathbf{Z}_l$	underlying linear system impedance
$\mathbf{Z}_n$	nonlinear system impedance
$\|\mathbf{Z}\|$	norm of matrix $\mathbf{Z}$
a	scalar perturbing coefficient
c_{ij}	viscous damping between nodes i and j
$\mathbf{f}$	excitation force
$\mathbf{f}_n$	internal force of nonlinear element
$h_{n_{ij}}$	(i,j) element of $\mathbf{H}_n$
k_{ij}	linear stiffness between nodes i and j
m_i	mass of ith DoF
r	number of frequency points
w	frequency dependent weighting coefficient
$\mathbf{x}$	minimum contribution of nonlinearity in nonlinear system response
$\mathbf{x}_o$	optimum equivalent linear system response
$\mathbf{x}_n$	nonlinear system response
x	relative displacement of two ends of nonlinear element
x_o	critical displacement of Jenkin's element
$\mathbf{\Delta H}$	difference between nonlinear and linear system FRFs
$\boldsymbol{\eta}_n$	nonlinear structural damping matrix

behavior and (c) be applicable for nonlinearities located at inaccessible/indeterminate degree of Freedoms (DoFs). To this end, the theory of "Optimum Equivalent Linear Frequency Response Function (FRF)" (OELF) [22] will be used and hence the proposed identification method is a frequency domain based method.

2. The theory of the optimum equivalent linear FRF

Fig. 1 shows a nonlinear system with force "f" as excitation and displacement "x_n" as response. The displacement time history will contain features due to nonlinearity which could not be produced by a linear system. Conceptually nonlinearities and noise are similar in as much as they both produce features in the response which could not be produced by a linear system.

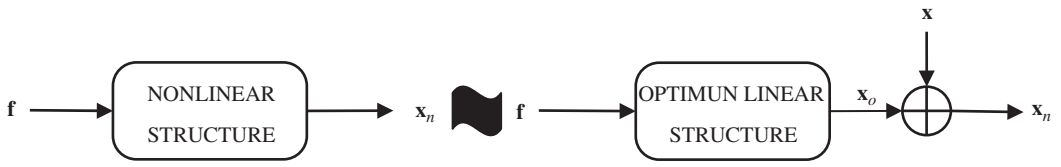

Fig. 1. Nonlinear and optimum equivalent linear system with corrected output.

The nonlinear system output may be replaced by an equivalent linear system output with a correction term added to it. The main goal of OELF method is to find an optimum model for equivalent linear system. In other words, if $\mathbf{x}$ is the part of nonlinear system response that is not supplied by the linear system, it is desired to find a linear system with response $\mathbf{x}_o$ that minimizes the effect of $\mathbf{x}$ in $\mathbf{x}_n$, i.e. $E[\mathbf{x}^2]$ must be reduced as much as possible. Frequency domain explanation of this requirement is as follows:

$$E[\mathbf{x}^2] = \int_{-\infty}^{+\infty} S_{\mathbf{xx}}(\omega)\,\mathrm{d}\omega = \int_{-\infty}^{+\infty} E\left[\frac{\mathbf{X}_n - \mathbf{X}_o}{T}\right]\mathrm{d}\omega \tag{1}$$

where $\mathbf{X}_0$ and $\mathbf{X}_n$ are the Fourier transform of $\mathbf{x}_o$ and $\mathbf{x}_n$, respectively. Now, let $\mathbf{H}_o(\omega)$ be the FRF matrix of equivalent linear model of the nonlinear system. Taking this definition into account, Eq. (1) can be written as follows:

$$E[\mathbf{x}^2] = \int_{-\infty}^{+\infty} E\left[\frac{\mathbf{X}_n - \mathbf{H}_o\mathbf{F}}{T}\right]\mathrm{d}\omega \tag{2}$$

Now, in order to find the optimum equivalent linear system that minimizes above integral, one has to find $\mathbf{H}_o(\omega)$ that minimizes this integral over the frequency range of interest and, considering $E[\mathbf{x}^2]$ as a functional, this can be done through the calculus of variations. To this end, let us assume that $\mathbf{H}_o(\omega)$ is the FRF of optimum equivalent linear system and is perturbed by $a\mathbf{G}(\omega)$ as in

$$\mathbf{H}_n(\omega) = \mathbf{H}_o(\omega) + a\mathbf{G}(\omega) \tag{3}$$

Here $\mathbf{G}(\omega)$ is defined as a frequency dependent function and a is a frequency independent scalar variable. Consequently Eq. (2) may now be written as follows:

$$\int_{-\infty}^{+\infty} S_{\mathbf{xx}}(\omega)\,\mathrm{d}\omega = \int_{-\infty}^{+\infty} E\left[\frac{|\mathbf{X}_n - (\mathbf{H}_o + a\mathbf{G})\mathbf{F}|^2}{T}\right]\mathrm{d}\omega \tag{4}$$

The nonlinearity effects may be minimized by taking the derivative of Eq. (4) with respect to a and setting the result to zero. Therefore the condition for the optimum linear equivalent FRF is

$$\int_{-\infty}^{+\infty} E\left[\frac{\mathbf{G}(\mathbf{X}_n^*\mathbf{F} - \mathbf{H}_o^*\mathbf{F}^*\mathbf{F}) + \mathbf{G}^*(\mathbf{X}_n\mathbf{F}^* - \mathbf{H}_o\mathbf{F}\mathbf{F}^*)}{T}\right]\mathrm{d}\omega = \mathbf{0} \tag{5}$$

* is used for conjugate transpose. Taking the expectation it is seen that this condition may be written as

$$\int_{-\infty}^{+\infty} E\left[\frac{\mathbf{G}(\mathbf{S}_{nf}^* - \mathbf{H}_o^*\mathbf{S}_{ff}) + \mathbf{G}^*(\mathbf{S}_{nf} - \mathbf{H}_o\mathbf{S}_{ff})}{T}\right]\mathrm{d}\omega = \mathbf{0} \tag{6}$$

Since $\mathbf{G}$ may be any function, each term in the integrand is zero. Finally, the optimum equivalent linear model for $\mathbf{H}_o(\omega)$ is described by

$$\mathbf{H}_o(\omega) = \mathbf{S}_{xf}\mathbf{S}_{ff}^{-1} \tag{7}$$

As is evident from Eq. (7), the OELF is derived simply by performing FFT calculations on the excitation and nonlinear response signals, and calculating the FRF function, as if we are dealing with a linear system input/output signals.

Also, if the variance of the excitation $\mathbf{F}$ is changed the spectral estimates of excitation and response will change in a non-proportional manner and, as Eq. (7) implies, a new $\mathbf{H}_o(\omega)$ will be calculated. This is a very important point and indicates that, for each level of excitation variance, an optimum equivalent liner model is calculated which is particular to that level of excitation.

From identification point of view, above conclusion means that OELF derived for each level of excitation carries some characteristic effects of the nonlinearity existing in the system with itself. It is this effect which will be used to identify the nonlinear mechanism in the system.

It is very important to note that damping of a nonlinear system may be described by OELF. Dissipated energy in frequency domain can be written as follows:

$$ED = \int_{-\infty}^{+\omega} \mathbf{S}_{\dot{x}f}\,\mathrm{d}\omega = \mathrm{i}\int_{-\infty}^{+\omega} \mathbf{H}_n\mathbf{S}_{ff}\omega\,\mathrm{d}\omega \tag{8}$$

Eq. (8) represents exact amount of the energy dissipated by nonlinear damping provided that the OELF used involves the force and displacement at nonlinearity location.

3. Identification process

Equation of motion for a MDoF system may be written as

$$\mathbf{M}\ddot{\mathbf{x}}_n + \mathbf{C}\dot{\mathbf{x}}_n + \mathbf{K}\mathbf{x}_n + \mathbf{f}_n(\mathbf{x}_n, \dot{\mathbf{x}}_n) = \mathbf{f} \tag{9}$$

Considering harmonic excitation and defining $\mathbf{Z}_n(\mathbf{X}_n, \dot{\mathbf{X}}_n)$ (in which $\dot{\mathbf{X}}_n$ is Fourier Transform of $\dot{\mathbf{x}}_n$) as the optimum equivalent linear impedance of the system (here in after called OELI), frequency domain representation of Eq. (9) can be written as Eq. (10) in which $\mathbf{Z}(\mathbf{X}_n, \dot{\mathbf{X}}_n)$ represents the optimum impedance of the nonlinear joint. Thus the OELI of system

for each level of excitation is the sum of linear and optimum linear joint contributions and can be written as:

$$-\omega^2\mathbf{M}+\mathrm{i}\omega\mathbf{C}+\mathbf{K}+\mathbf{Z}(\mathbf{X}_n,\dot{\mathbf{X}}_n)=\mathbf{Z}_n \tag{10}$$

The above statement and resulted Eq. (10) are, in concept, very similar to impedance derived from the first-order harmonic balance.

The aim of present work is to identify $\mathbf{Z}(\mathbf{X}_n,\dot{\mathbf{X}}_n)$ for each and every level of random excitation and, in this respect, two different methods are introduced, namely, 1—Direct and; 2—Model based, impedance Identification Methods (DIM and MIM, respectively). Both methods will be discussed and examined in details.

3.1. Direct impedance identification

Examination of Eq. (10) implies that the $\mathbf{Z}(\mathbf{X}_n,\dot{\mathbf{X}}_n)$ may be derived from direct subtraction of the overall OELI and the impedance of underlying linear system (zero-order impedance). This approach, being theoretically very simple, presents some difficulties in practical identification work as the impedances are very difficult to measure. To get around this problem, Eq. (10) will be reformulated in Eq. (13) using the technique introduced in [23] which was mainly used as a finite element model updating technique for linear structures:

$$\mathbf{Z}=\mathbf{Z}_n-\mathbf{Z}_l \tag{11}$$

Rewriting this equation with FRF matrices $\mathbf{Z}_n=\mathbf{H}_n^{-1}$ and $\mathbf{Z}_l=\mathbf{H}_l^{-1}$ will have the following consequence:

$$\mathbf{Z}=\mathbf{H}_n^{-1}-\mathbf{H}_l^{-1}=\mathbf{H}_n^{-1}\mathbf{H}_l\mathbf{H}_l^{-1}-\mathbf{H}_n^{-1}\mathbf{H}_n\mathbf{H}_l^{-1} \tag{12}$$

Eq. (12) rearrangement leads to Eq. (13) in which no impedance is used except for that of the optimum equivalent joint impedance:

$$\mathbf{H}_n\mathbf{Z}\mathbf{H}_l=\mathbf{H}_l-\mathbf{H}_n=-\Delta\mathbf{H} \tag{13}$$

3.1.1. Transformation into standard form

The next step is to convert Eq. (13) into a standard form. In the standard form $\mathbf{Z}$ is converted to a vector that contains rows of $\mathbf{Z}$. Consequently, right hand side of Eq. (13) is expressed in vector form too. Finally, new format of Eq. (13) is

$$\underbrace{\begin{bmatrix}\ddots & \vdots & \iddots\\ \cdots & h_{n_{i,j}}\mathbf{H}_l^T & \cdots\\ \iddots & \vdots & \ddots\end{bmatrix}}_{\mathbf{A}(\omega)}\underbrace{\begin{Bmatrix}\vdots\\ \mathbf{Z}_{j,:}^T\\ \vdots\end{Bmatrix}}_{\mathbb{Z}}=-\underbrace{\begin{Bmatrix}\vdots\\ \Delta\mathbf{H}_{j,:}^T\\ \vdots\end{Bmatrix}}_{\mathbf{B}(\omega)} \tag{14}$$

In which subscripts i,j, j,: and superscript T mean ijth element, jth row and transpose of related matrix, respectively. Selection of ith row of $\mathbf{H}_n$ and jth column of $\mathbf{H}_l$ is corresponding to kth row ($k=(i-1)N+j$, where N is the assumed number of DoFs) of Eq. (14). The flow diagram for the DIM is presented in Fig. 2.

3.2. Model based impedance identification

Going back to Eq. (14) again, following models are defined for $\mathbf{Z}$ and introduced in Eq. (15):

$$\mathbf{Z}(\overline{X})=\begin{cases}\mathbf{K}_n(\overline{X})+\mathrm{i}\omega\mathbf{C}_n(\overline{X}) & \text{for viscous damping}\\ \mathbf{K}_n(\overline{X})+\mathrm{i}\boldsymbol{\eta}_n(\overline{X}) & \text{for hystertic damping}\end{cases} \tag{15}$$

where $\overline{X}$ designates RMS(x) in Eq. (15). As can be seen from Eq. (15), the nonlinear stiffness and damping are considered as depending on RMS of response. As indicated in Section 2, this is due to the fact that OELI (or OELF) are derived for each level of random excitation RMS value and this in turn directly corresponds to a specific response RMS value. Therefore, in

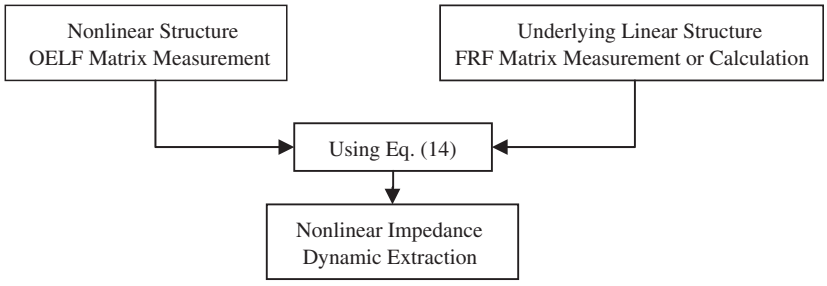

Fig. 2. DIM flow diagram.

frequency domain nonlinearity may be described as a function of displacement RMS and this can be related to amplitude of an equivalent harmonic signal as $X = \sqrt{2}\mathrm{RMS}(x)$. So, the nonlinear stiffness and loss factors can be related to the amplitude of a harmonic excitation.

3.2.1. Frequency weighting

Depending on the physical nature of nonlinearity, high level of fluctuations is observed in OELFs for some excitation levels. High level excitation for cubic stiffness nonlinearity and low level one for pure slip and stick-slip will lead to this situation. These fluctuations in OELFs lead to erroneous results. To overcome this problem, equations are weighted along the frequency axis. Weighting coefficient at each frequency is selected as $\|\Delta\mathbf{H}\|^{-1}$. Finally, Eq. (16) will be the weighted form of Eq. (14) where $\mathbb{Z}$ in Eq. (16) is introduced in Eq. (14):

$$\underbrace{w(\omega)\mathbf{A}(\omega)}_{\mathbf{P}(\omega)}\mathbb{Z} = \underbrace{-w(\omega)\mathbf{B}(\omega)}_{\mathbf{Q}(\omega)} \tag{16}$$

3.2.2. Least square problem

After weighting, in accordance with measured components of $\mathbf{H}_n$, rows of Eq. (16) are selected at r frequency points and this will lead to a least square equation as in

$$\begin{bmatrix} \begin{bmatrix} \mathbf{P}_{i,:}(\omega_1) \\ \vdots \\ \mathbf{P}_{i,:}(\omega_r) \end{bmatrix} \\ \vdots \\ \begin{bmatrix} \mathbf{P}_{k,:}(\omega_1) \\ \vdots \\ \mathbf{P}_{k,:}(\omega_r) \end{bmatrix} \end{bmatrix} \mathbb{Z} = \begin{bmatrix} \begin{bmatrix} \mathbf{Q}_{i}(\omega_1) \\ \vdots \\ \mathbf{Q}_{i}(\omega_r) \end{bmatrix} \\ \vdots \\ \begin{bmatrix} \mathbf{Q}_{k}(\omega_1) \\ \vdots \\ \mathbf{Q}_{k,:}(\omega_r) \end{bmatrix} \end{bmatrix} \tag{17}$$

The flow diagram for the MIM is presented in Fig. 3.

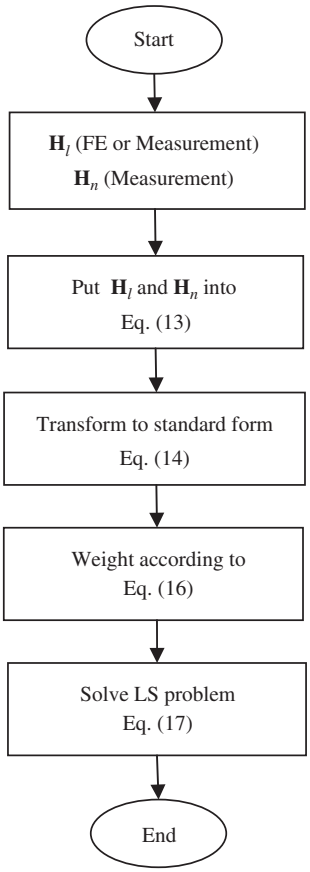

Fig. 3. MIM flow diagram.

4. Case studies, results and discussions

To examine the efficiency of the proposed method, series of case studies are considered. However, before considering the case studies, it is important to clarify what is exactly meant by "joint" in this paper, in order to justify the models considered in the case studies. Generally speaking, by joint we mean part of a structure or system that connects adjacent components and/or structures that may or may not impose constraints on connecting degrees of freedom and, most important of all, joints are much localized, i.e. relatively taking small proportion of the total degrees of freedom of the system. The latter characteristic means that a joint behavior is very much location dependent and, for example, a joint may have a significant linear or nonlinear effect on vibration behavior of a structure in one mode and much less effect or non for the others.

With the definition given above in mind, the word joint can cover a broad span from adhesives to weld and of course this means that significantly different values could be assigned to the characteristics of the joint in the case studies. The values chosen are typical and are only serving for the purpose of demonstrating the efficiency of the proposed method.

4.1. System description

A 4DoF system is considered for all of the case studies. Fig. 4 shows this system. A nonlinear element is attached to the system between ground and first DoF. The other components of the system are assumed to be linear viscous damping and stiffness. Three types of nonlinearities are involved: (a) Cubic Stiffness (CS), (b) Pure Slip (PS), and (c) Stick-Slip (SS). Coulomb model is considered for friction and SS is modeled by a Jenkins element which is shown schematically in Fig. 5. The value of system parameters are listed in Table 1.

4.2. MAC analysis between modes from different methods

In order to assess that how well OELF describes the behavior of the nonlinear system compared to other methods, mode shapes are estimated from the OELF for three types of the nonlinearities mentioned above at low and high RMS level of excitations. In order to do this, system shown in Fig. 4 is subjected to pseudo random excitation and then equations of motions are solved and OELF matrix is calculated using Eq. (7) and FFT analysis. In next step, modal analysis is performed on OELFs by ICATS [24] modal analysis software.

The mode shapes extracted as above will be compared to the mode shapes which are derived directly from time history of the response. In this respect, system is excited by a harmonic signal with a frequency very close to the nonlinear resonances. Normalized displacement vector at an arbitrary time exhibits the related mode shape. This method is

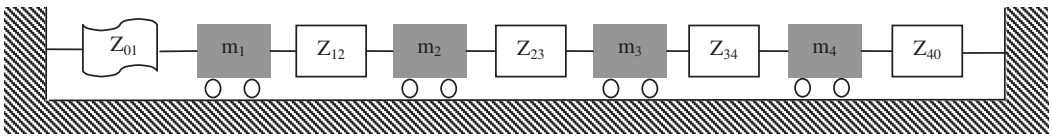

Fig. 4. Nonlinear structure.

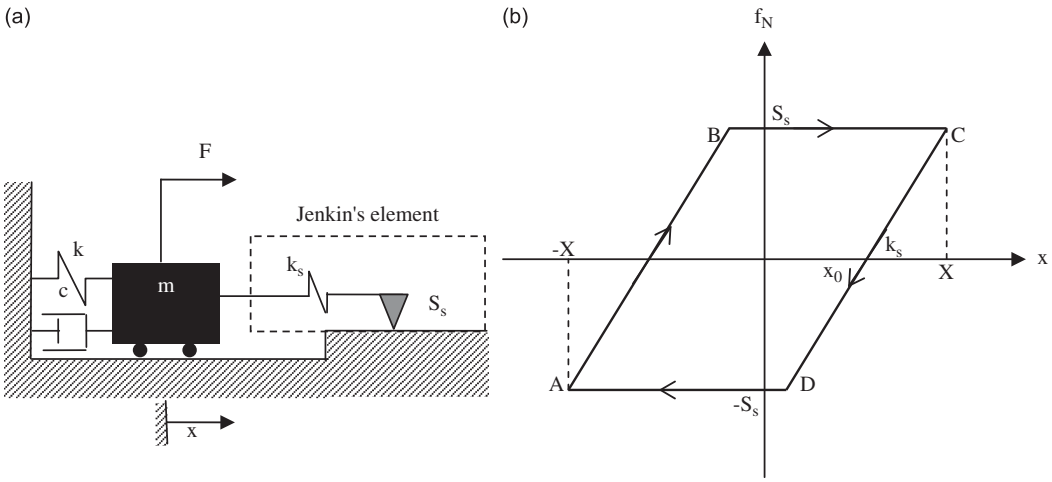

Fig. 5. (a) Jenkin's element for stick-slip modeling and (b) Jenkin's element force–displacement relation.

designated as TD (time domain). In order to ensure that same amount of energy is transmitted to the system by the excitation, the RMS values of responses for the pseudo random and harmonic excitations are kept in the same level. The TD technique is used as a reference as it gives the most direct description of the first-order frequency response function of the system. This is due to the fact that in deriving the first-order FRF with this method no assumptions are involved and the time domain signal is directly used for the FRF estimation. This also means less numerical errors in calculations. It should

Table 1
System parameters values.

Mass (kg)				
m_1	m_2	m_3	m_4	
1	1	1	1	
Viscous damping (kg/s)				
c_{01}	c_{12}	c_{23}	c_{34}	c_{40}
0.01	0.01	0.01	0.01	0.01
Linear stiffness (N/m)				
k_{01}	k_{12}	k_{23}	k_{34}	k_{40}
1000	800	900	700	900
Cubic stiffness (N/m^3)				
K_{301}	K_{312}	K_{323}	K_{334}	K_{340}
10^7	0	0	0	0
Pure slip friction force (N)				
P_{s01}	P_{s12}	P_{s23}	P_{s34}	P_{s40}
0.1	0	0	0	0
Jenkin's stiffness (N/m)				
K_{s01}	K_{s12}	K_{s23}	K_{s34}	K_{s40}
1000	0	0	0	0
Jenkin's friction force (N)				
S_{s01}	S_{s12}	S_{s23}	S_{s34}	S_{s40}
1	0	0	0	0

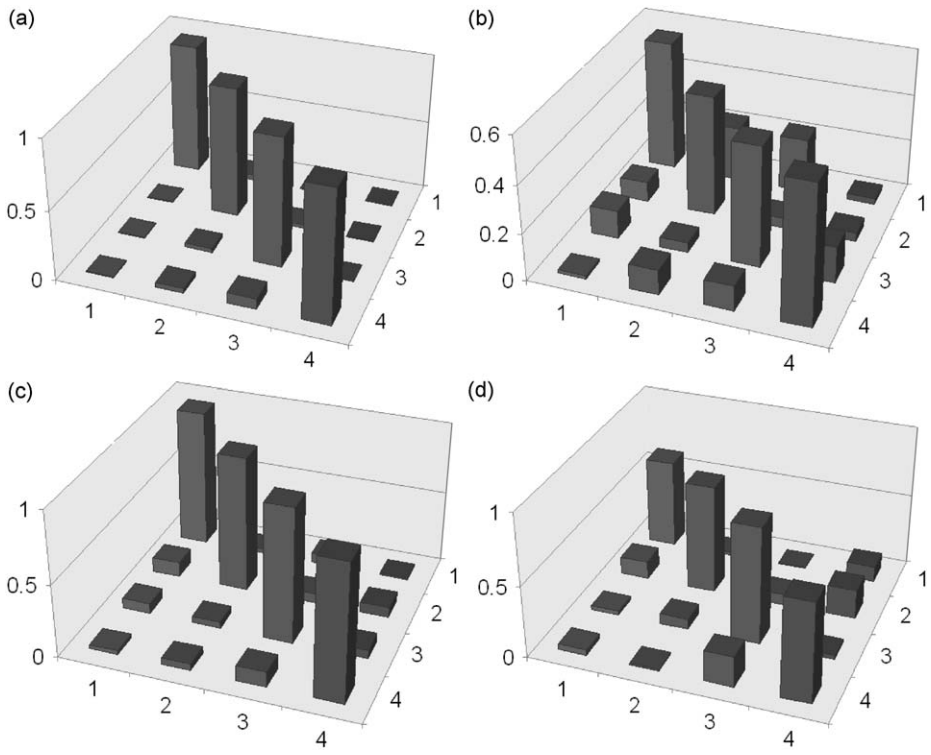

Fig. 6. MAC analysis for CS nonlinearity, (a) and (b) MAC (NLSRM and OELF), low and high excitation level, respectively; (c) and (d) MAC (TD and OELF), low and high excitation level, respectively.

be noticed, however, that nonlinear system response to a harmonic signal contains sub and super harmonics of excitation and therefore the response will not be pure harmonic but, at least for weakly nonlinear systems, sub and super harmonics' contributions in response are much smaller than main component hence, TD extracted modes are close to the real ones.

The third set of mode shapes which will be used for the comparison purpose is derived from Nonlinear Single Resonant Mode (NLSRM) [25,26] method. In its present context, this method is only applicable for CS nonlinearity.

Fig. 6 shows the MAC results for CS nonlinearity. The first row displays correlation between modes estimated from OELF and NLSRM at two different modal amplitudes. The second row contains the MAC for TD and OELF. This figure shows that there is a good accordance between results. In fact, a better correlation can be seen between OELF and TD than NLSRM and TD which indicates that OELF gives a more accurate description of the nonlinear system modal behavior for CS nonlinearity.

MAC analysis results for PS nonlinearity are presented in Fig. 7. Again a fair amount of agreement exists here, too. It is worth noticing that for this case the correlation is increased with modal amplitude increment which indicates a smaller friction effect as the excitation level increases. This is in accordance with the results derived from HBM [27,28].

For the SS nonlinearity MAC result are shown in Fig. 8 which indicates a very good correlation between results.

Therefore, OELF proves to be a proper frequency-domain model of a nonlinear system at a specific level of excitation, at least, as far as the three types of nonlinearities considered are involved.

4.3. Direct identification method results

Impedances of identified CS nonlinearity at three excitation levels are shown in Fig. 9. Nonlinearity lies between ground and m_1 therefore, only m_1 displacement can excite the nonlinearity. As is evident from this figure, the first element of identified impedance matrix has significant values in comparison with other. In fact, all elements except that of first row have negligible value. Next, the second nonlinearity type, PS, is investigated by direct method. In this case, results are shown as real and imaginary parts instead of magnitude and phase as this presentation is more meaningful for PS. Due to its damping effect, imaginary part of impedance is more important for this type of nonlinearity. Imaginary part of **Z** is

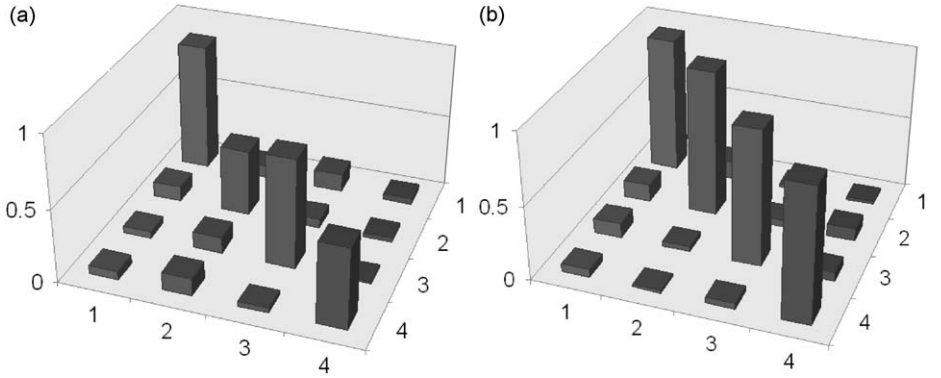

Fig. 7. MAC analysis for PS nonlinearity, (a) and (b) MAC (TD and OELF), low and high level excitation, respectively.

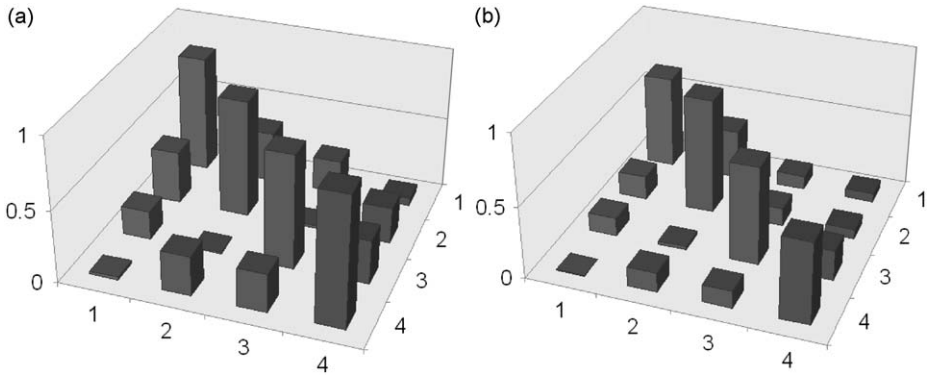

Fig. 8. MAC analysis for SS nonlinearity, (a) and (b) MAC (TD and OELF), low and high level excitation, respectively.

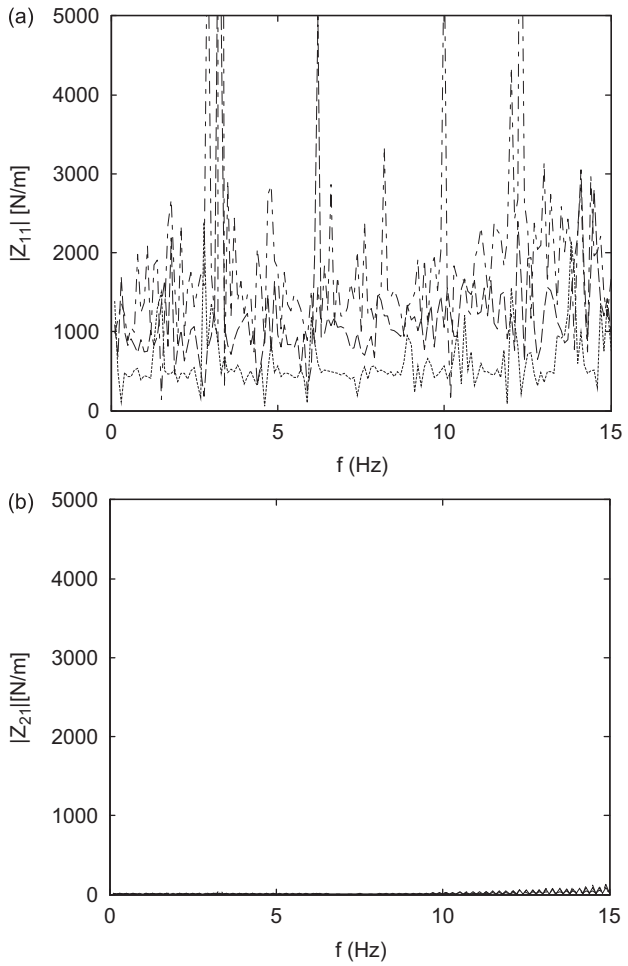

Fig. 9. Magnitude of estimated **Z** by DIM for CS nonlinearity: (a) $|\mathbf{Z}(1,1)|$, (b) $|\mathbf{Z}(2,1)|$, – – $\sigma_F = 0.350$ N, —— $\sigma_F = 0.606$ N, – · – $\sigma_F = 0.870$ N.

displayed in Fig. 10. As expected, first element of **Z** has signs of nonlinearity. Finally, real and imaginary parts of complex dynamic stiffness **Z** for SS nonlinearity are shown in Fig. 11.

This result demonstrates the existence of nonlinearity in system. Also, the difference between identified results for different excitation level is an indication of the system nonlinearity.

It is worth mentioning that for the both DIM and MIM the linear (zero order) FRF may be measured for CS and SS nonlinearities by low level excitation and for PS nonlinearity by high level excitations. The linear FRF matrix can also be derived from an accurate FE model and this method has advantages over measurement of linear FRF as it is not easy to measure linear FRFs for PS and SS nonlinearities.

It is inferred form above studies that the nonlinearity existence and location may be identified but quantifying would be very tedious by DIM.

4.4. Model based identification method results

The parameters $\mathbf{K}_n$ and $\boldsymbol{\eta}_n$ in Eq. (15) are identified here. In order to assess the efficiency of the process, constraints will be imposed on **Z** one at a time. Consequently, **Z** is assumed: 1—to be Constraint-Free (CF), 2—to be SyMmetric (SM), 3—to have special Connectivity Pattern (CP), 4—to be Symmetric and to have special Connectivity pattern (SC) and 5—to have a configuration in which nonlinearity has Specified Location (SL).

Also, due to the similarity between optimum equivalent impedance of the nonlinear system derived by Harmonic Balance Method (HBM) with OELI in Eq. (10), the impedances derived by HBM for three nonlinear elements used in the case studies will be compared with those identified by Eq. (17). Impedances derived by HBM for three considered nonlinearities are displayed in Table 2. HBM has been employed to predict nonlinear impedance of some nonlinearities such as CS and PS in many texts. But SS nonlinearity has not been considered in any publication to the authors' knowledge. This problem is investigated in appendix.

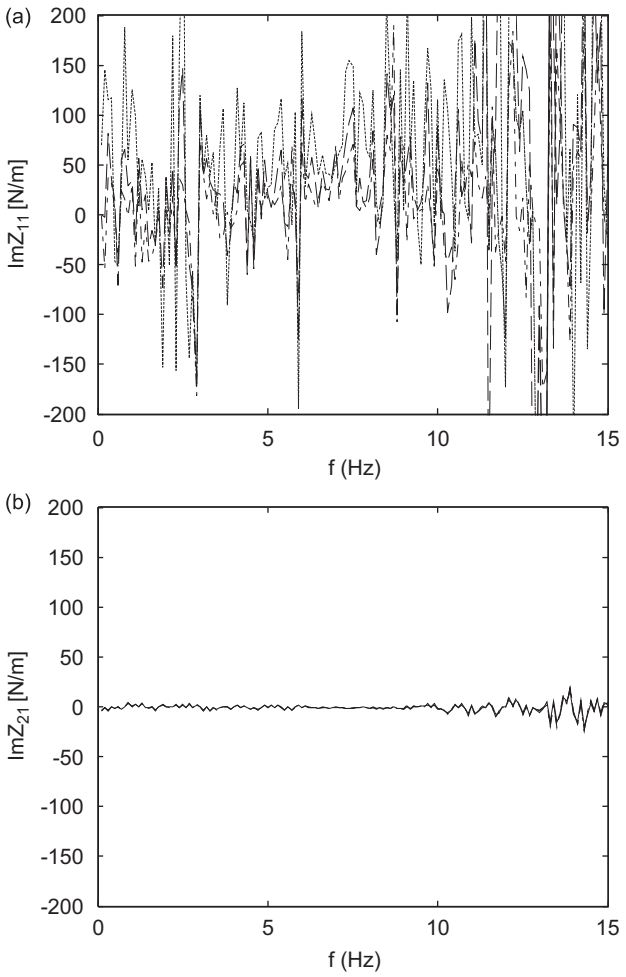

Fig. 10. Imaginary part of estimated **Z** by DIM for PS nonlinearity: (a) Im($\mathbf{Z}(1,1)$), (b) Im($\mathbf{Z}(2,1)$), – –$\sigma_F = 0.520$ N, —— $\sigma_F = 0.780$ N, – · – $\sigma_F = 1.040$ N.

4.4.1. Cubic stiffness

Fig. 12 shows the identified $\mathbf{K}_n$ for CS nonlinearity. In these figures only first element has been displayed to maintain brevity. $\mathbf{K}_{n_{11}}$ is the most important element of above matrices as nonlinearity is located between ground and m_1. As expected this stiffness term increases with RMS(x). As is evident, although the best correlation between identified stiffness and HBM is achieved when either complete $\mathbf{H}_n$ matrix or the first row of it is used in identification process, nevertheless, fair amount of correlation exist between two set of parameters even when other rows of $\mathbf{H}_n$ is used in identification. In Figs. 12a and b results related to CF constraint are more similar to HBM results.

The other identified elements of $\mathbf{K}_n$ matrix (which do not exist in reality) are several order of magnitude smaller than the $\mathbf{K}_{n_{11}}$ and can be easily spotted and ignored. These identified elements can be attributed to inaccuracy in FFT analysis in deriving the OELF matrix as well as the other numerical errors.

It is worth mentioning that, due to nonlinear effects, time signals are non-symmetric, and consequently OELF matrix will not be symmetric either. This non-symmetry can also be observed in identified parameters. As mentioned in the beginning of this section, part of the results is identified with symmetry enforced on the $\mathbf{K}_n$ matrix, in order to examine its effects on the identified parameters.

4.4.2. Pure slip

Estimated $\boldsymbol{\eta}_n$ for PS nonlinearity are presented in Fig. 13. As expected, $\mathbf{K}_n$ has no significant meaning because PS has no stiffness effects. Equivalent damping coefficient decreases as displacement RMS increases. In this case like previous one entire $\mathbf{H}_n$ and $\mathbf{H}_n(1,:)$ give better correlated results using different assumptions.

4.4.3. Stick-slip

Before reaching the displacement of m_1 to the sliding threshold of Jenkins element, the discrepancy between underlying linear system and nonlinear one is k_s. In fact, system behaves linearly in this region. Sliding threshold i.e. $x_o = ss_{01}/ks_{01}$ is

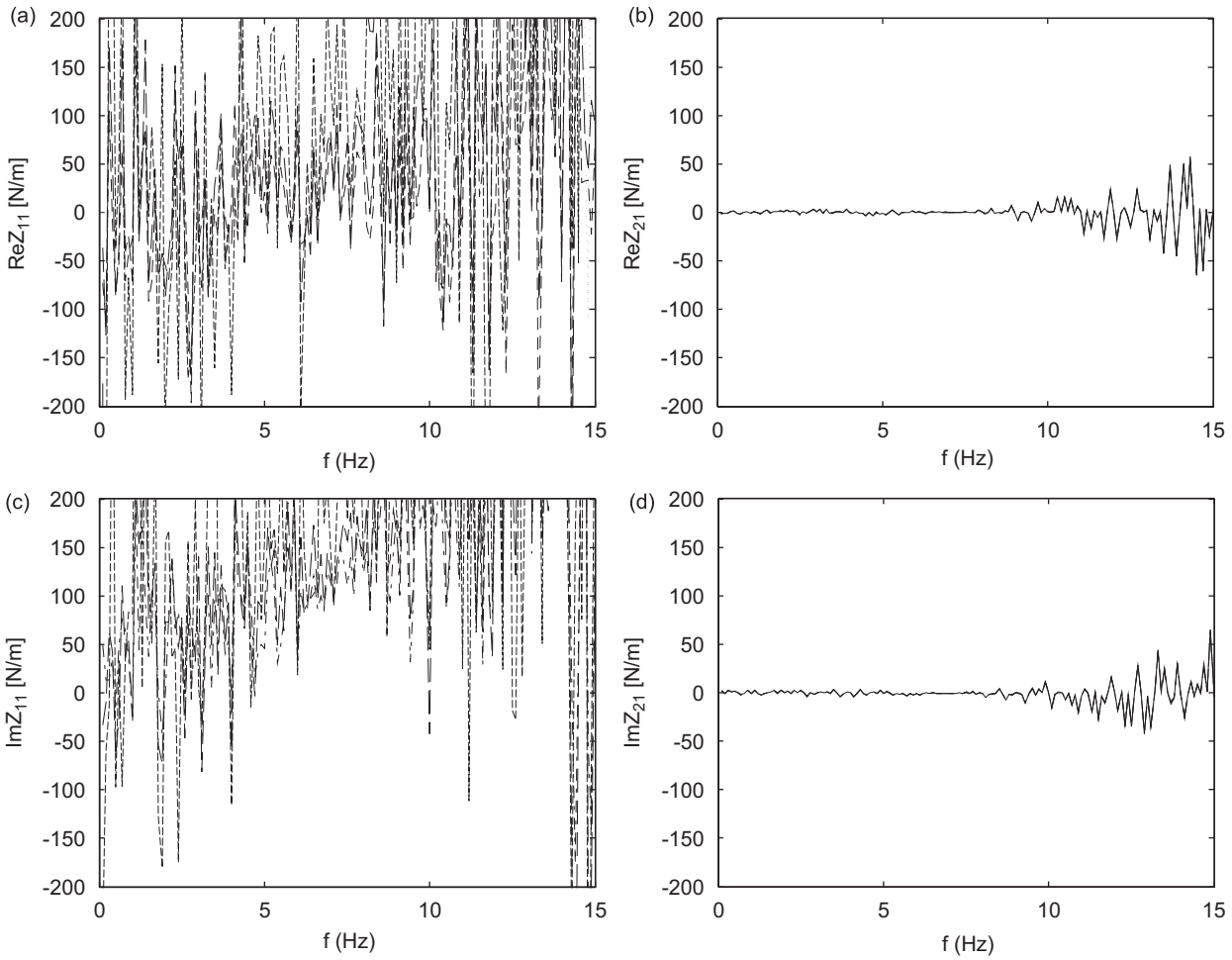

Fig. 11. Real and imaginary parts of estimated **Z** by DIM for SS nonlinearity: (a) Re($\mathbf{Z}(1,1)$), (b) Re($\mathbf{Z}(2,1)$), (c) Im($\mathbf{Z}(1,1)$), (d) Im($\mathbf{Z}(2,1)$) – – $\sigma_F = 3.460$ N, —— $\sigma_F = 6.060$ N, – · – $\sigma_F = 8.660$ N.

Table 2
HB prediction for impedance of three nonlinearity types.

Nonlinearity	K_n	η_n
Cubic stiffness	$\frac{3}{4}k_3X^2$ [a]	
Pure slip		$\frac{4}{\pi}\frac{p_s}{X}$
Stick-slip	$\frac{4(2s_s - k_sX)\sqrt{s_s(k_sX - s_s)} + k_s^2X^2(\pi + 2\beta)}{2\pi k_sX^2}$ [b]	$\frac{4s_s(k_sX - s_s)}{\pi k_sX^2}$

[a] X is the response amplitude.

[b] $\beta = \sin^{-1}\left(\frac{2s_s}{k_sX} - 1\right)$.

equal to 1 mm with our selected parameters and the excitation levels has been chosen such that it is ensured that the nonlinear element is excited.

Identified first elements of matrices $\mathbf{K}_n$ and $\boldsymbol{\eta}_n$ are shown in Fig. 14. Outcomes of employing entire $\mathbf{H}_n$ are presented in Fig. 14a and the rest parts of the figure include results derived by using individual rows. The most important element of above matrices is the first i.e. $\mathbf{K}_{n_{11}}$ and $\boldsymbol{\eta}_{n_{11}}$ using either entire $\mathbf{H}_n$ or $\mathbf{H}_n(1,:)$, the agreement between estimated $\mathbf{K}_{n_{11}}$ and $\boldsymbol{\eta}_{n_{11}}$ with various constraints imposed with each other and with HBM is good.

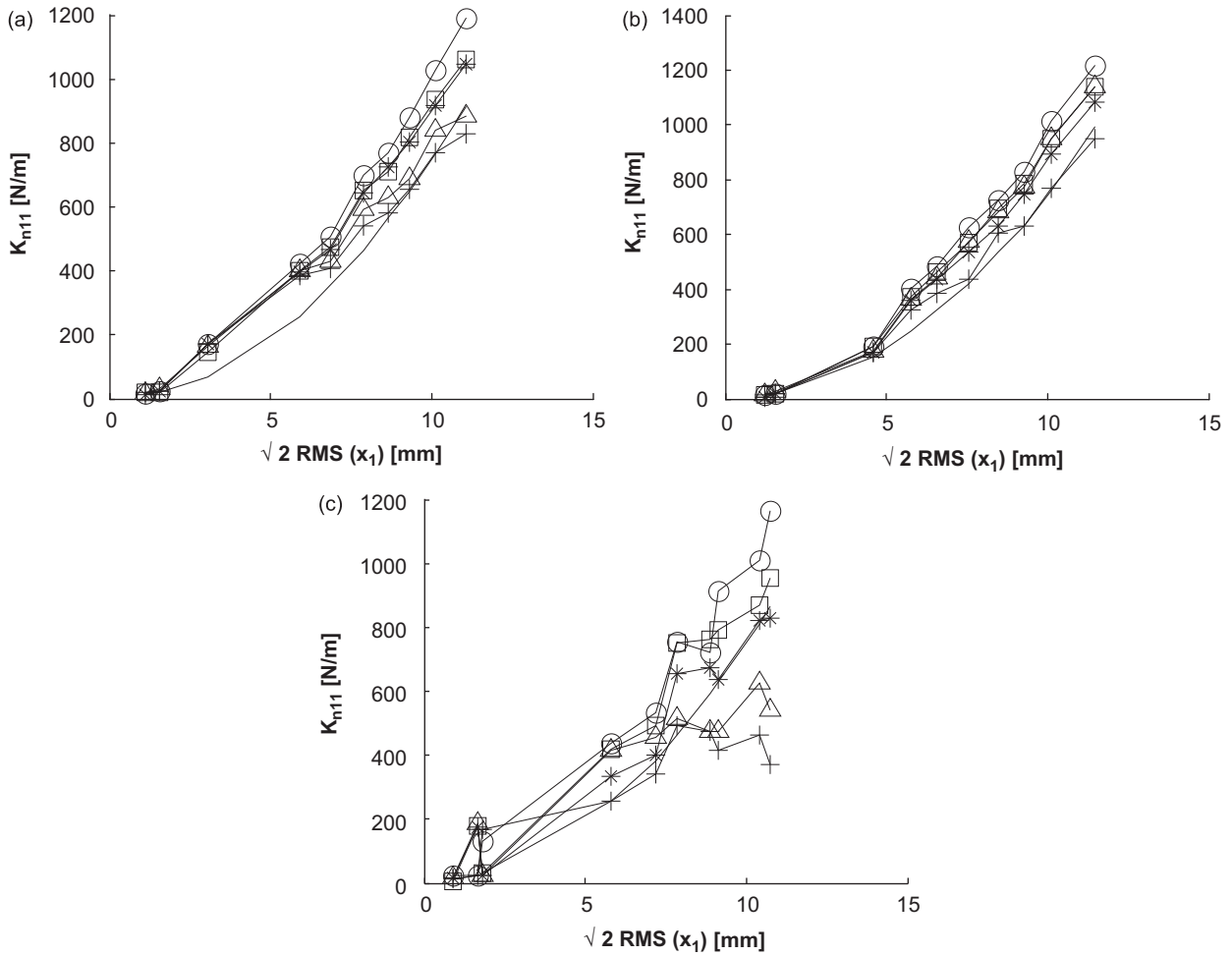

Fig. 12. CS nonlinearity identification by MIM using: (a) entire $\mathbf{H}_n$, (b) 1st row of $\mathbf{H}_n$, (c) 2nd row of $\mathbf{H}_n$, — HB,+CF, × SM, △ CP, □ SC, ○ SL.

In numerical solution of equation of motion, integration time steps should be very small, in order to be able to adequately model the parallelogram shape of force–displacement diagram (Fig. 5b). Here, time step is set to be about the inverse of 10 times of greatest system natural frequency. Consequently, exact shape of force–displacement diagram is not considered. On the other hand, HBM models the parallelogram shape of force–displacement diagram with an elliptic. These to different non-exact modeling cause some difference between identified parameters and HBM results especially, for identified damping.

Estimation of $\mathbf{K}_{n_{11}}$ and $\boldsymbol{\eta}_{n_{11}}$ using other rows of $\mathbf{H}_n$ leads to less accurate results though the general trend correlation is still acceptable. This is more noticeable for damping coefficient. As expected, nonlinear stiffness is reduced by increasing RMS(x) and hence the system has softening behavior. After a preliminary and brief increase, growth of RMS(x) reduces the damping coefficient.

4.5. Response regeneration

The identified nonlinear parameters are incorporated in the model and, assuming a harmonic excitation, the amplitude spectrum matrix of the response is calculated using an iterative solution procedure similar to HBM. Fig. 15 exposes the comparison between such calculated amplitude spectrums with those calculated from HB, first-order FRF and OELF.

5. Practical considerations

Existence of matrix $\mathbf{H}_n$ in the left hand side of Eq. (13) implies that OELJ matrix, $\mathbf{Z}$, can be estimated only at coordinates for which $\mathbf{H}_n$ can be measured. In practice, nonlinearity may be located at inaccessible/indeterminate DoFs, e.g. rotational

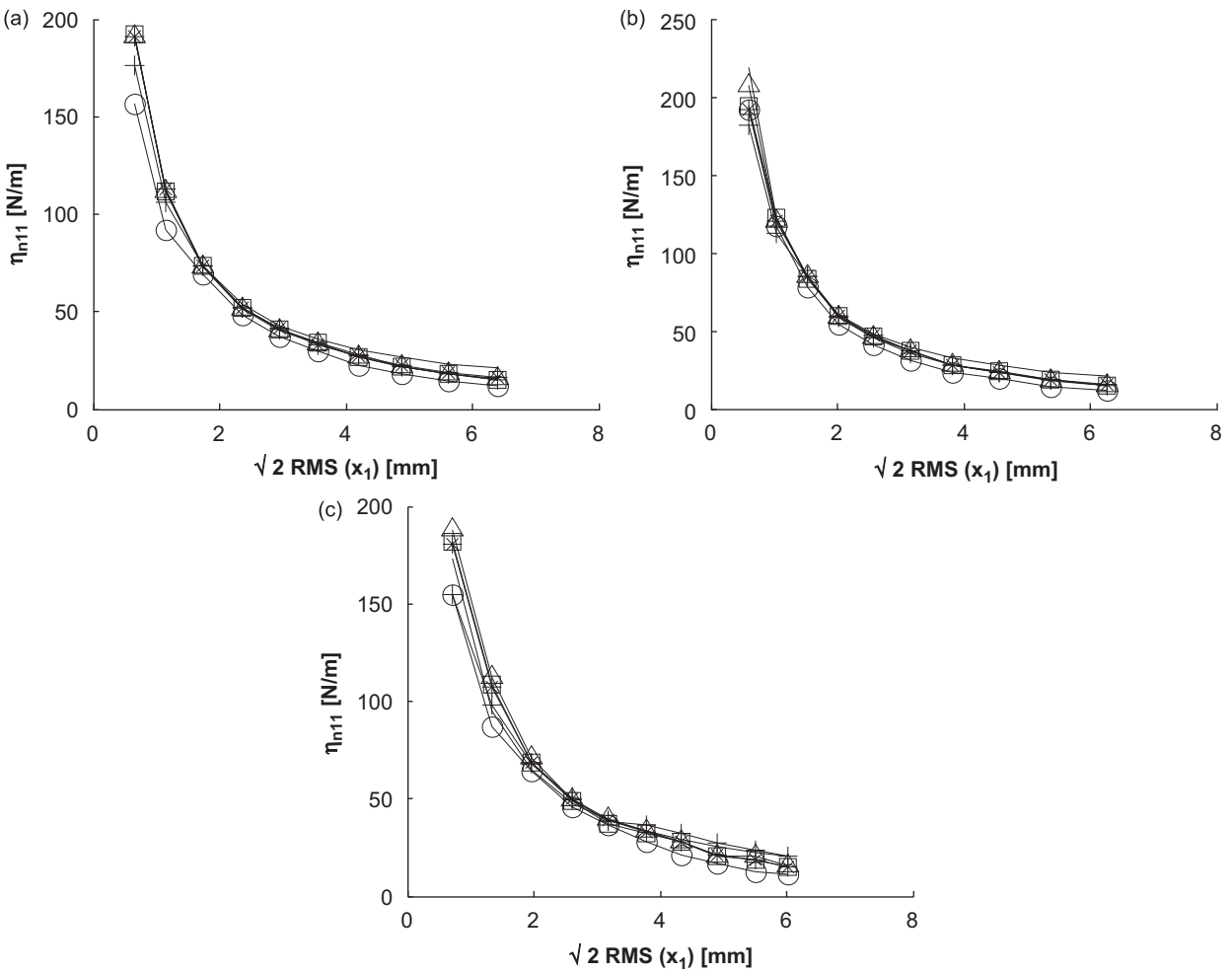

Fig. 13. PS nonlinearity identification by MIM using: (a) entire $\mathbf{H}_n$, (b) 1st row of $\mathbf{H}_n$, (c) 2nd row of $\mathbf{H}_n$, — HB,+CF, × SM, △ CP, □ SC, ○ SL.

DoFs or, locations which are not accessible to mount sensor and hence $\mathbf{H}_n$ cannot be measured for those DoFs. Therefore, to eliminate this limitation another form of Eq. (13) is introduced, as follows.

Lets $\mathbf{H}_l$ be the FRF matrix of underlying linear system which may be determined easily by FEM. Model obtained form FEM can have any DoFs either translational or rotational ones. Now, the perturbation based version of Eq. (13) can be derived as follows:

$$\mathbf{Z}_n = \mathbf{Z}_l + \mathbf{Z}$$

$$\mathbf{H}_n = (\mathbf{Z}_l + \mathbf{Z})^{-1}$$

$$\mathbf{H}_n = \mathbf{H}_l - \mathbf{H}_l\mathbf{Z}\mathbf{H}_l + O(\mathbf{Z}^2) \tag{18}$$

Terms $O(\mathbf{Z}^2)$ in Eq. (18) will be negligible if $\Delta\mathbf{H}$ is small. Therefore, Eq. (13) may be reformed to

$$\mathbf{H}_l\mathbf{Z}\mathbf{H}_l \approx -\Delta\mathbf{H} \tag{19}$$

Now, while only measured coordinates are present on the right hand side of Eq. (19), any desired OELJ matrix that adequately represents the active DoFs of joint may be considered on the left hand side of Eq. (19).

Due to non-exact characteristic of Eq. (19), it should be solved iteratively and after each iteration step $\mathbf{H}_l$ is updated to $\mathbf{H}_{l_{new}} = (\mathbf{H}_{l_{old}}^{-1} + \mathbf{Z})^{-1}$. This process ends when $\mathbf{Z}$ calculated in ith step is small enough and/or $\Delta\mathbf{H}$ becomes very small. Accumulation of estimated impedances of overall process will be the desired identified OLEJ impedance.

Iteration process of solving Eq. (19) may experience difficulties if $\|\Delta\mathbf{H}\|$ is big and in this situation, relaxation techniques prove to be very helpful. In this respect the $\|\Delta\mathbf{H}\|$ is reduced artificially by considering a proportion of real $\mathbf{H}_n$ on the right

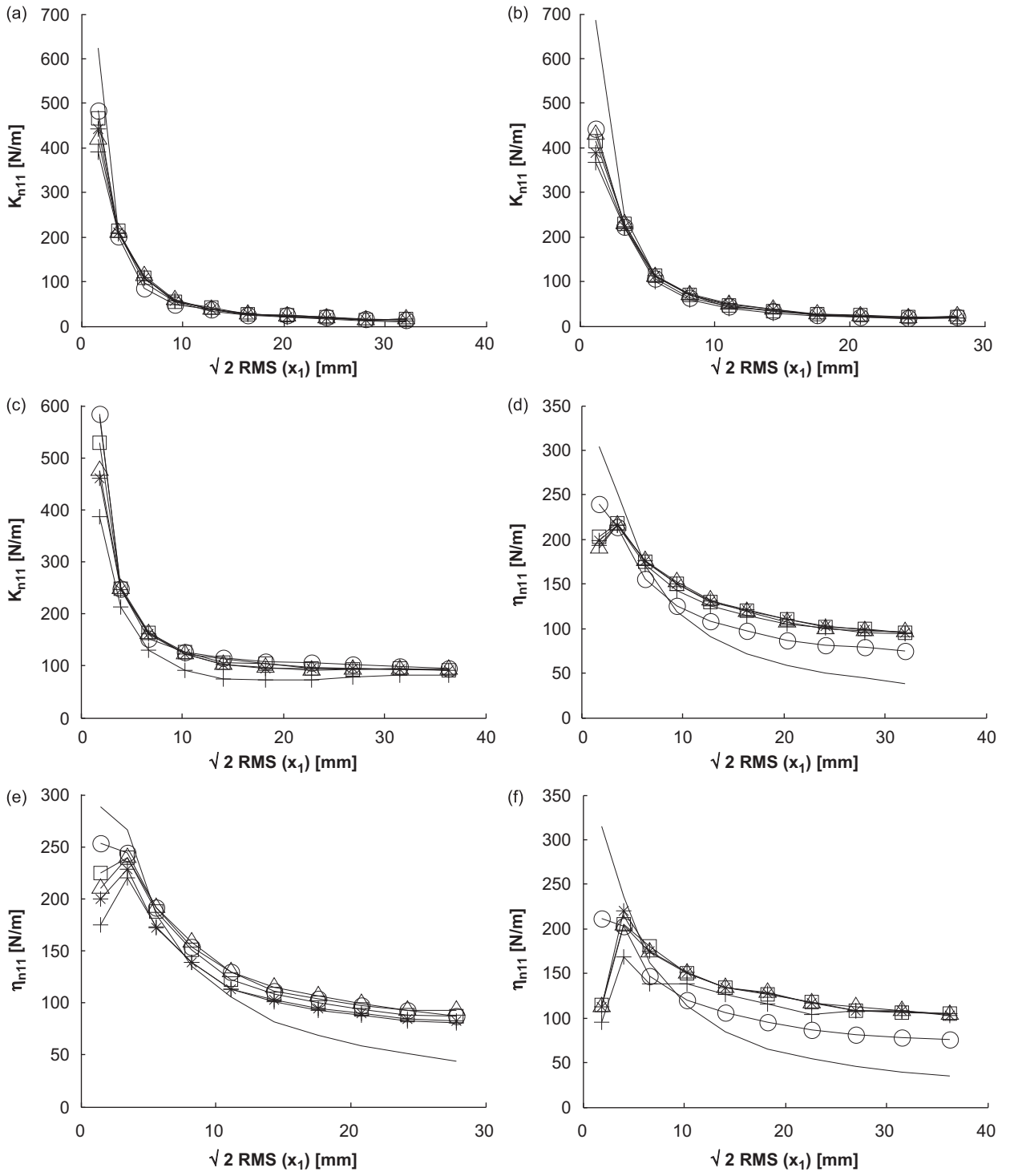

Fig. 14. SS nonlinearity identification by MIM using: (a) and (d) entire $\mathbf{H}_n$, (b) and (e) 1st row of $\mathbf{H}_n$, (c) and (f) 2nd row of $\mathbf{H}_n$, — HB,+CF, × SM, △ CP, □ SC, ○ SL.

hand side of Eq. (19). After convergence is achieved on this portion then the real $\mathbf{H}_n$ will be used in a second round of the solution.

The rest of the procedure would be the same as that used in Eqs. (14)–(17) and, as mentioned above, here Eq. (17) must be solved iteratively. Fig. 16 shows the flow diagram of modified MIM.

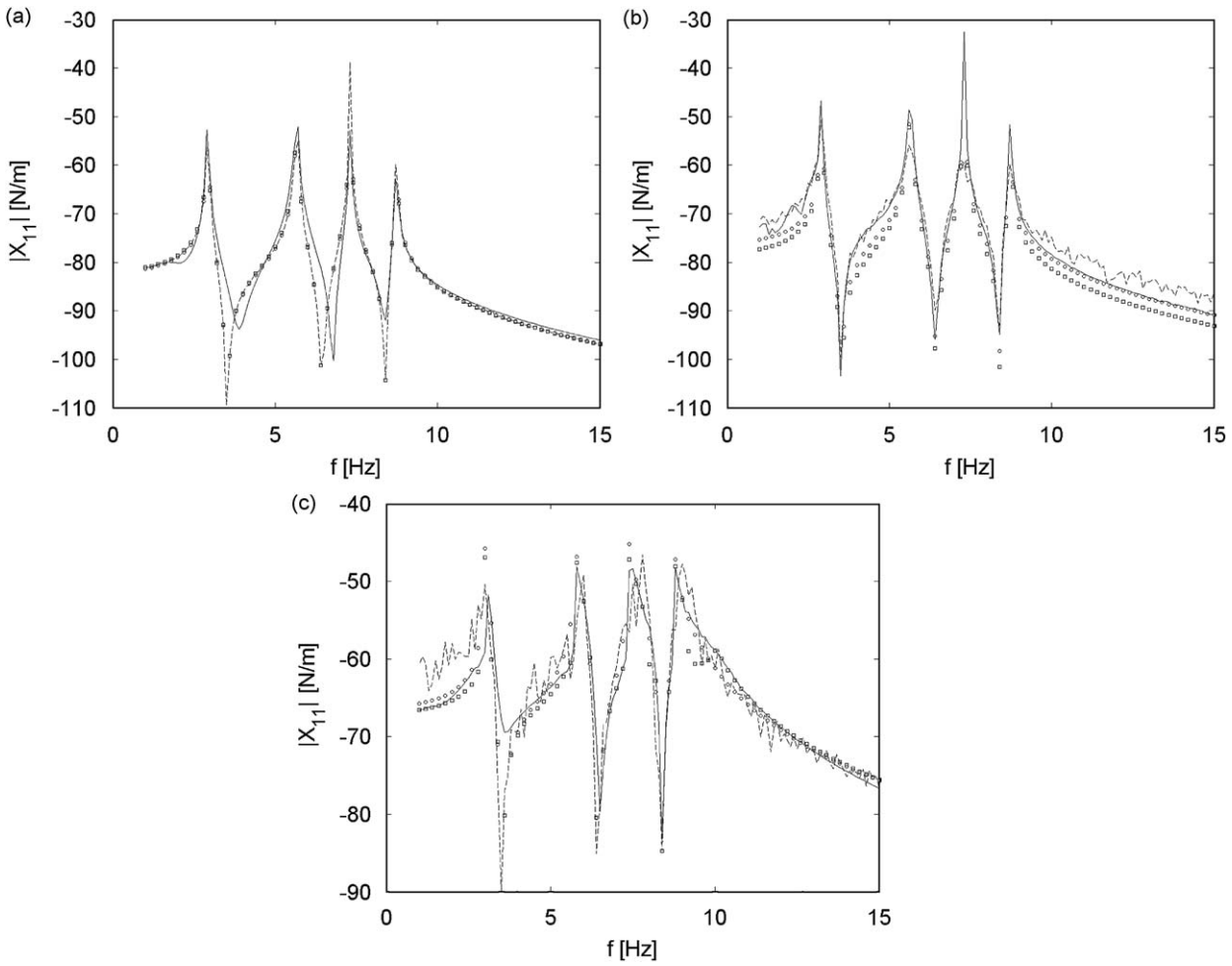

Fig. 15. Regenerated response at 1st DoF due to excitation at same DoF: (a) CS, (b) PS, (c) SS, — harmonic excitation, – – pseudo-random excitation, □ HBM, ○ identification results.

5.1. Case studies

The same system used in Section 4, will be used to demonstrate the efficiency of the method based on Eq. (19). It is worth mentioning that in all case studies explained below only part of the matrix $\mathbf{H}_n$ is exploited in calculations and the rest of the elements of this matrix are considered as indeterminate.

5.1.1. Cubic stiffness

Fig. 17 shows the parameter identified using Eq. (19) and three last elements of second column of $\mathbf{H}_n$. Fair amount of correlation exist between results at low response RMSs but for high response RMSs this formulation fails to identify CS nonlinearity except for CP and SC constraints. The other identified elements of $\mathbf{K}_n$ matrix (which do not exist in reality) are several order of magnitude smaller than the $\mathbf{K}_{n_{11}}$ and can be easily spotted and ignored. As before, these identified elements can be attributed to inaccuracy in FFT analysis in deriving the OELF matrix as well as the other numerical errors.

5.1.2. Pure slip

Estimated $\boldsymbol{\eta}_n$ for PS nonlinearity are shown in Fig. 18. As before, only element (1,1) of matrix $\boldsymbol{\eta}_n$ have been displayed. Here, three last elements of second columns of $\mathbf{H}_n$ are used for Eq. (19). Equivalent damping coefficient decreases as displacement RMS increases. Results have a good agreement with HBM. In this case, nonlinearity reduces as response RMS increases and so, results consistency will improve.

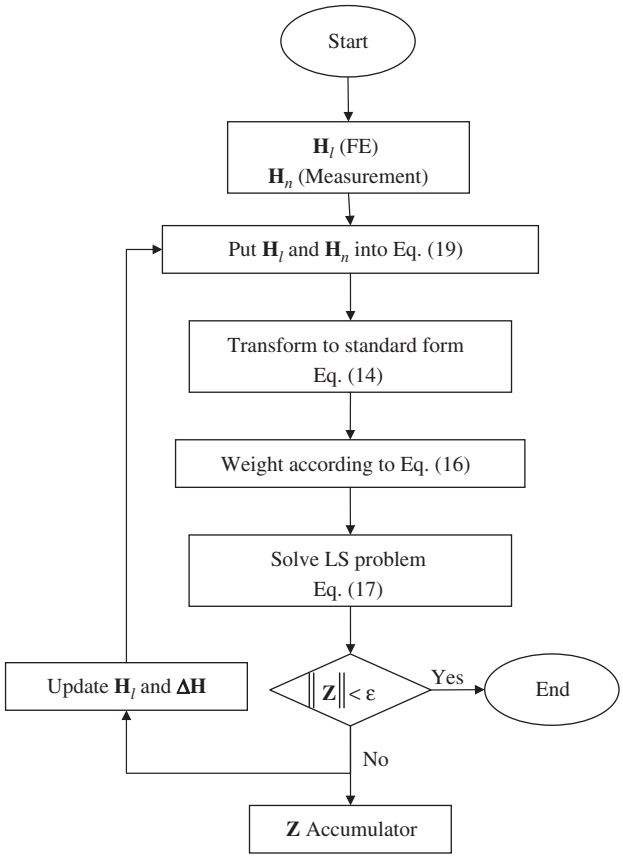

Fig. 16. Flow diagram of modified MIM.

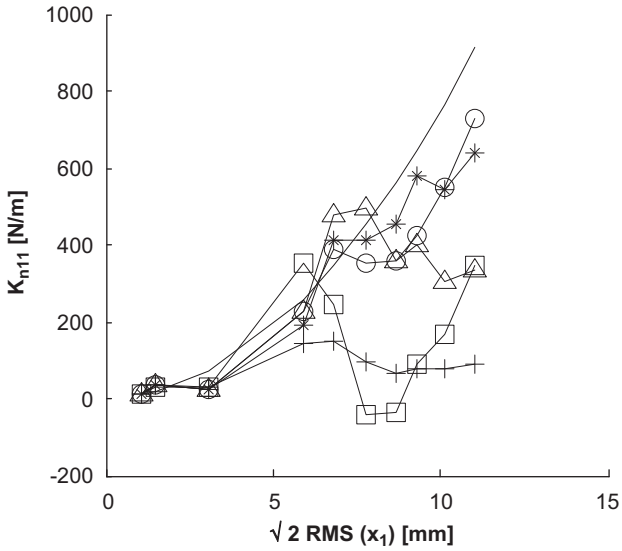

Fig. 17. Estimated $\mathbf{K}_{n_{11}}$ for CS using modified MIM: — HB, □ CF, △ SM, ○ CP, ∗ SC,+SL.

5.1.3. Stick-slip

Element (1,1) of identified nonlinear stiffness and damping matrices are shown in Fig. 19 using Eq. (19). As in the previous cases, three last elements of second columns of $\mathbf{H}_n$ are used. The agreement between estimated $\mathbf{K}_{n_{11}}$ and $\boldsymbol{\eta}_{n_{11}}$, with

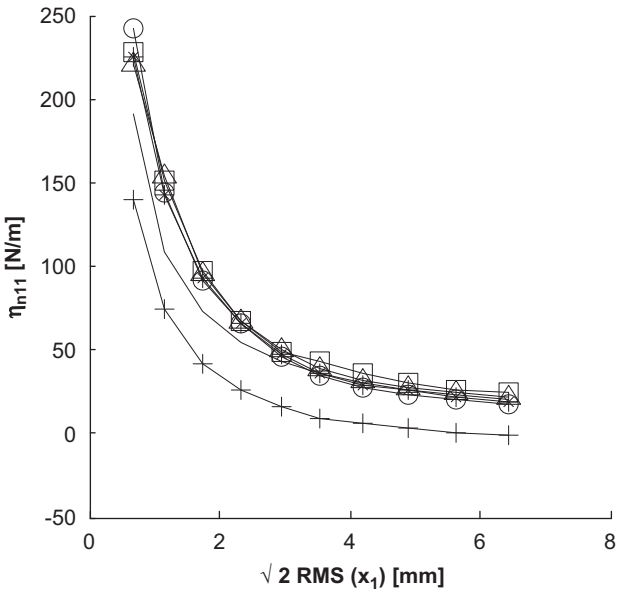

Fig. 18. Estimated $\eta_{n_{11}}$ for PS using modified MIM: — HB, □ CF, △ SM, ○ CP, ∗ SC,+SL.

various constraints imposed, with HBM is good. As mentioned in MIM results, some of the differences between identified results and HB estimation can be attributed to the fact that in HBM a perfect parallelogram is assumed to estimate impedance while, in simulated identification process this situation does not exist. As is expected, nonlinear stiffness is reduced by increasing RMS(x) and hence the system has softening behavior. Also, increase in RMS(x) reduces the damping coefficient.

6. Conclusion

A general method was proposed for identification of nonlinear dynamics joint characteristics. It was shown that method is simple and straight forward and does not require sophisticated experimental setup and yet can be efficiently applied to three most important types of nonlinear mechanisms in dynamic analysis. Modified version of identification method was introduced to consider the practical limitations such as indeterminable/inaccessible DoFs. This version is able to identify nonlinearities even without measurement or excitation at nonlinearity location.

It is also demonstrated that the harmonic balance method and the proposed method are closely related and in fact, as far as the nonlinear impedance of the joint is concerned, they are identical. The method can handle both viscous and hystertic damping models and can be easily extended to identification of frequency dependent nonlinear joints.

Appendix A. HBM prediction for SS nonlinearity impedance

HBM has been employed to predict nonlinear impedance of some nonlinearities such as CS and PS in many texts. But SS nonlinearity has been not considered in any publication to the authors' knowledge. This problem is investigated here. In Fig. 5a displacement of mass is considered to be harmonic as

$$x(t) = X\sin(\omega t - \varphi) \tag{A.1}$$

Angular position of points A…D in Fig. 5b can be obtained with considering Eq. (A.2) as follows:

$$-X = X\sin(\omega t_A - \varphi) \Rightarrow \omega t_A - \varphi = 2k'\pi - \frac{\pi}{2}$$

$$X = X\sin(\omega t_C - \varphi) \Rightarrow \omega t_C - \varphi = 2k'\pi + \frac{\pi}{2} \tag{A.2}$$

In which $k' = 0, \pm 1, \pm 2, \pm 3, \ldots$ and, for point B determined angular position is expressed by

$$-X + 2x_o = X\sin(\omega t_B - \varphi) \Rightarrow \omega t_B - \varphi = 2k'\pi + \sin^{-1}\left(2\frac{x_o}{X} - 1\right) = 2k'\pi + \beta \tag{A.3}$$

Finally, point D has π radians shift relative to point B, i.e. $\omega t_D - \varphi = \beta + \pi$. Fig. 20 describes the position and relation of mentioned points on unit trigonometric circle.

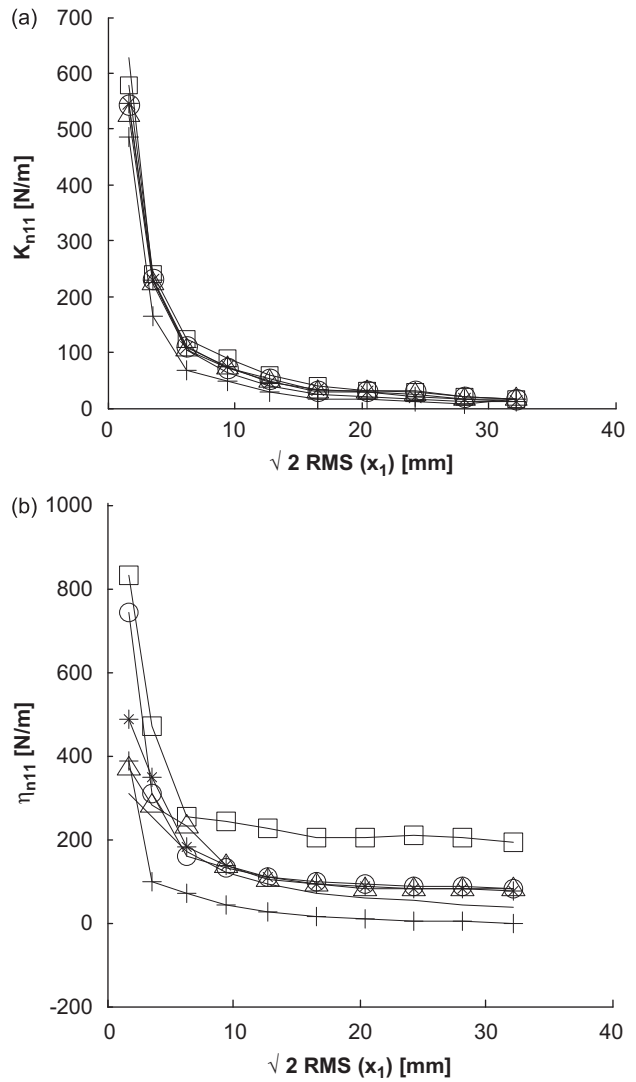

Fig. 19. Estimated parameters for SS using modified MIM: (a) $\mathbf{K}_{n_{11}}$, (b) $\boldsymbol{\eta}_{n_{11}}$, — HB, □ CF, △ SM, ○ CP, ∗ SC,+SL.

As response, the force of Jenkin's element is considered to be harmonic as follows:

$$f_{ss}(t) \simeq a^* \cos \omega t + b^* \sin \omega t \tag{A.4}$$

Eq. (A.4) in fact is the first harmonic term of Fourier expansion. Its coefficient may be calculated by either Fourier relationships or Galerkin's method, however, two methods are totally similar and their result is summarized in

$$a^* = \frac{2}{T}\int_0^{\mathrm{T}} f_{ss}(x(t))\cos \omega t \, \mathrm{d}t$$

$$b^* = \frac{2}{T}\int_0^{\mathrm{T}} f_{ss}(x(t))\sin \omega t \, \mathrm{d}t \tag{A.5}$$

Breaking the interval of integral according to angular position of points A…D on the unit trigonometric circle and taking all of the resultant integrals leads one to the following expressions for a^* and b^*:

$$a^* = -\frac{4(2S_s - k_sX)\sqrt{S_s(k_sX - S_s)} + k_s^2X^2(\pi + 2\beta)}{2\pi k_sX}\sin\varphi + \frac{4S_s(k_sX - S_s)}{\pi k_sX}\cos\varphi$$

$$b^* = +\frac{4S_s(k_sX - S_s)}{\pi k_sX}\sin\varphi + \frac{4(2S_s - k_sX)\sqrt{S_s(k_sX - S_s)} + k_s^2X^2(\pi + 2\beta)}{2\pi k_sX}\cos\varphi \tag{A.6}$$

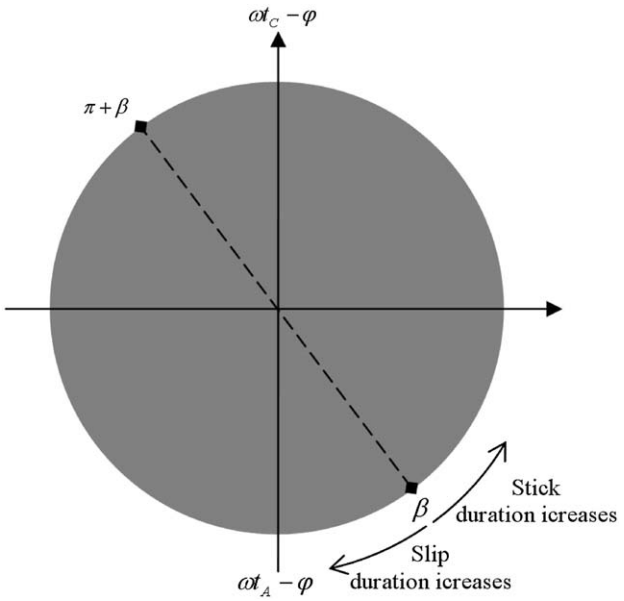

Fig. 20. Stick-slip switching points of Jenkin's element on unit trigonometric circle.

Substituting Eq. (A.6) in equation of motion and comparing with the linear impedance definition, give HB estimated impedance of Jenkin's element. This impedance is as follows:

$$Z = \frac{4(2S_s - k_s X)\sqrt{S_s(k_s X - S_s)} + k_s^2 X^2(\pi + 2\beta)}{2\pi k_s X^2} + \mathrm{i}\frac{4S_s(k_s X - S_s)}{\pi k_s X^2} \tag{A.7}$$

References

[1] K. Jahani, A.S. Nobari, Identification of dynamic (Young's andshear) moduli of a structural adhesive using modal based direct model updating method, *Experimental Mechanics* (2008) 599–611, doi:10.1007/s11340-008-9131-7.
[2] J.R.F. Arruda, S.H.S. Carneiro, Experimental estimation of mechanical joint parameters using frequency response function and modal parameters, *Proceedings IMAC* (1993) 1502–1507.
[3] W.L. Li, A new method for structural model updating and joint stiffness identification, *Mechanical Systems and Signal Processing* 16 (1) (2002) 155–167.
[4] M.J. Ratcliffe, N.A.J. Lieven, A generic element-based method for joint identification, *Mechanical Systems and Signal Processing* 14 (1) (2000) 3–28.
[5] K.T. Yang, Y.S. Park, Joint structural parameter identification using a subset of frequency response function measurement, *Mechanical Systems and Signal Processing* 7 (6) (1993) 509–530.
[6] J.H. Wang, S.C. Chaung, Reducing errors in the identification of structural joint parameters using error functions, *Journal of Sound and Vibration* 273 (1–2) (2004) 295–316.
[7] F. Thouverez, L. Jezequel, Identification of a localized non-linearity, *International Journal of Non-Linear Mechanics* 33 (1998) 935–939.
[8] D.M. Storer, G.R. Tomlinson, Recent developments in the measurements and interpretation of higher order functions from nonlinear structures, *Mechanical Systems and Signal Processing* 7 (1993) 173–189.
[9] A. Chatterjee, N.S. Vyas, Non-linear parameter estimation through Volterra series using the method of recursive iteration through harmonic probing, *Journal of Sound and Vibration* 268 (2003) 657–678.
[10] A. Chatterjee, N.S. Vyas, Non-linear parameter estimation in multi-degree-of-freedom systems using multi-input Volterra series, *Mechanical Systems and Signal Processing* 18 (2004) 457–489.
[11] G. Kerschen, K. Worden, A.F. Vakakis, J.C. Golinval, Past, present and future of nonlinear system identification in structural dynamics, *Mechanical System and Signal Processing* 20 (2006) 505–592.
[12] K. Yasuda, S. Kawamura, K. Watanabe, Identification of nonlinear multi-degree-of-freedom systems (presentation of an identification technique), *JSME International Journal Series III* 31 (1988) 8–14.
[13] K. Yasuda, S. Kawamura, K. Watanabe, Identification of nonlinear multi-degree-of-freedom systems (identification under noisy measurements), *JSME International Journal Series III* 31 (1988) 302–309.
[14] M. Thothadrai, R.A. Casas, F.C. Moon, R. D'Andrea, C.R. Johnson, Nonlinear system identification of multi-degree-of-freedom systems, *Nonlinear Dynamics* 32 (2003) 307–322.
[15] M. Thothadrai, F.C. Moon, Nonlinear system identification of systems with periodic limit-cycle response, *Nonlinear Dynamics* 39 (2005).
[16] H.J. Rice, J.A. Fitzpatrick, The measurement of nonlinear damping in single-degree-of-freedom systems, *Journal of Vibration and Acoustics* 113 (1991) 132–140.
[17] H.J. Rice, J.A. Fitzpatrick, A procedure for the identification of linear and non-linear multi-degree-of-freedom systems, *Journal of Sound and Vibration* 149 (1991) 397–411.
[18] C.M. Richards, R. Singh, Identification of multi-degree-of-freedom non-linear systems under random excitations by the reverse-path spectral method, *Journal of Sound and Vibration* 213 (1998) 673–708.
[19] J.A. Fitzpatrick, H.J. Rice, Comments on identification of multi-degree-of-freedom non-linear systems under random excitations by the 'reverse path' spectral method, *Journal of Sound and Vibration* 237 (2000) 357–358.
[20] D.E. Adams, R.J. Allemang, A frequency domain method for estimating the parameters of a non-linear structural dynamic model through feedback, *Mechanical Systems and Signal Processing* 14 (2000) 637–656.

[21] M.R. Hajj, J. Fung, A.H. Nayfeh, S. Fahey, Damping identification using perturbation techniques and higher-order spectra, *Nonlinear dynamics* 23 (2000) 189–203.
[22] H.G.D. Goyder, *Short Course Notes: Vibration Analysis and Identification of Nonlinear Structures*, University of Manchester, Simon Engineering Laboratories, NY, 1985.
[23] R.M. Lin, D.J. Ewins, Model updating using FRF Data, *15th International Modal Analysis Seminar*, Leuven, Belgium, 1990, pp. 141–163.
[24] ICATS Manual, Imperial College of Science, Technology and Medicine, Mechanical Engineering Department, Exhibitation Road, London SW7 2BX, 1994.
[25] W. Szemplinska-Stupnicka, The modified single mode method in the investigation of the resonant vibrations of nonlinear systems, *Journal of Sound and Vibration* 63 (1979) 475–489.
[26] A.S. Nobari, M. Shahramyar, Improvement of nonlinear single resonant mode method, *Journal of Vibration and Acoustic* 125 (2003) 59–63.
[27] M.E. Ozer, H.N. Ozgüven, T.J. Royston, Identification of structural non-linearities using describing functions and Sherman–Morrison method, *Proceedings of the 23rd International Modal Analysis Conference*, Orlando, 2005.
[28] A.H. Nayfeh, D.T. Mook, *Nonlinear Oscillations*, Wiley-Interscience, New York, 1979.